CHERENKOV-TYPE TERAHERTZ GENERATION IN SI-PRISM-LINBO3-SLAB STRUCTURE PUMPED BY NANOJOULE-LEVEL ULTRASHORT LASER PULSES

E.A. Mashkovich, M.I. Bakunov, M.V. Tsarev, S.D. Gorelov

Nizhny Novgorod State University

Optical rectification of ultrashort laser pulses in electrooptic crystals is an established way to generate broadband terahertz radiation. The most promising generation schemes include tilted-pulse-front pumping of a prism-shaped $LiNbO_3$ (LN) crystal [1] and Cherenkov radiation from a LN optical slab waveguide sandwiched between two Si prisms (or a prism and a substrate) [2]. By using tens-of-mJ-level amplified laser systems, the tilted-pulse-front pumping technique has recently resulted in generation of near-single-cycle terahertz pulses with energies as high as 125 μJ [3]. The sandwich-type scheme with a thin LN slab shows the highest optical-to-terahertz conversion efficiency for tens-of-μJ-level optical pumping. In the proof-of-principle experiment [4], the efficiency over 0.1% was achieved by converting 40 μJ Ti:sapphire laser pulses in 8mm long Si-LN-BK7 structure with a 50 μm thick LN core into terahertz pulses of ~3 THz bandwidth. In this experiment, only the terahertz beam emitted from the output Si prism was collected by the detector, about half of the generated terahertz energy was absorbed in the BK7-glass substrate. Recently, an improved design of the sandwich structure with a totally reflected substrate − a metal plate separated from the LN slab by an air gap − was proposed [5]. Using such a substrate allows one to concentrate the terahertz emission in one direction (into the output Si prism) and, furthermore, to tune the maximum of the terahertz spectrum by varying the width of the air gap. A record conversion efficiency of 0.25% was achieved for 15–20 μJ Ti:sapphire laser pulses in 1 cm long Si-LN-air-metal structure with a 35 μm thick LN core [6].

Here we are investigating the radiation geometry from the sandwich-type structure pumped by unamplified laser pulses of nJ-level. This scheme of THz generation allows one to achieve two orders of magnitude higher conversion efficiency as compared to the widely used collinear phase-matching scheme of THz generation in ZnTe [7].

Physically, the operating conditions of the sandwich-type optical-to-terahertz convertor are significantly different for the amplified and unamplified pumping regimes. In the amplified pumping regime, [4, 6] the optical beam is focused by a cylindrical lens into a line parallel to the plane of the sandwich structure. Focusing into a line is used for several reasons, but it can not be applied to the case of unamplified laser pumping. To provide a high optical intensity required for nonlinear optical rectification, the laser beam should be focused to a size ≤100 μm in the plane of the structure. This drastically changes the radiation geometry from two-dimensional to three-dimensional and, therefore, leads to a divergence of the generated terahertz beam (Cherenkov cone).

To calculate terahertz emission from the sandwich structure, we generalize the 2D approach developed in [2] and [5] to the 3D problem under consideration. The generation scheme we used for our calculations is shown in Fig. 1. A slab of 1% MgO-doped stoichiometric LN of a 35 μm thickness (along the x-axis) and 10 × 10 mm^2 lateral dimensions (in the y, z-plane) was bonded to a right triangular high-resistivity-Si prism cut at the Cherenkov angle 41^0.

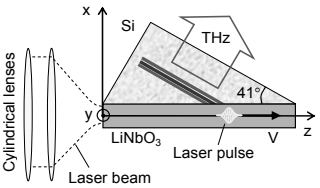

Fig. 1

Figure 2 shows the spatial distribution of the calculated electric field Ey at a fixed moment of time in two planes of the sandwich structure. In the calculation, we put pulse duration τ_{FWHM} = 100 fs, transverse size l_{YFWHM} = 50 μm, and the pump pulse energy Wopt = 8nJ. In the plane y=0 (Fig. 2(a)), the opening angle of the Cherenkov cone in Si is about 41^0. The gradually fading oscillations in the field distribution across the Cherenkov cone can be attributed to multiple reflections of the generated in the LN slab terahertz waves at the slab boundaries. Due to total internal reflection at the LN-air interface, the THz field experiences a fast exponential decay in the air. In the plane z=8.75 mm (i.e., 1.15 mm behind the laser pulse centered at z=9.9 mm) (Fig. 2(b)), the distribution of the radiation field over the cone is strongly inhomogeneous: the field is concentrated in the upper part of the cone and impinges on the Si-air interface (x≈1.1 mm in Fig. 2(b)) at small angles.

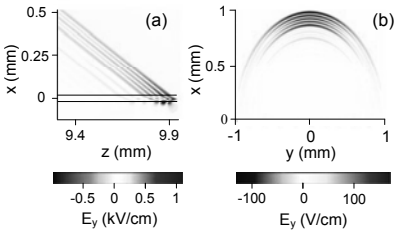

Fig. 2

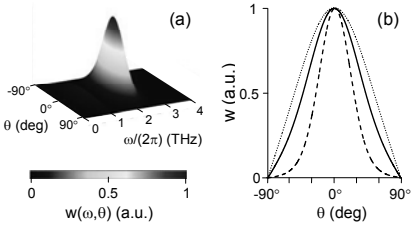

Fig. 3

Figure 3 (a) shows the spectral-angular density of terahertz energy w(ω,θ). There is a peak at θ=0^0 and ω/2π≈2 THz. The width of the peak along the θ-axis increases with reducing l_{YFWHM} and equals ~50, ~85, and ~100^0 for l_{YFWHM}=100, 50, and 25 μm, respectively (Fig.3(b)).

[1] Hebling J., Almasi G., Kozma I. Z., Kuhl J. //Opt. Express. 2002. V.10. P.1161.
[2] Bodrov S.B., Bakunov M.I., Hangyo M. //J. Appl. Phys. 2008. V.104. P.093105.
[3] Fulop J.A., Palfalvi L., Klingebiel S. et al. //Opt. Lett. 2012. V.37. P.557.
[4] Bodrov S.B., Stepanov A.N., Bakunov M.I. et al. //Opt. Express. 2009. V.17. P.1871.
[5] Bakunov M.I., Bodrov S.B. //Appl. Phys B. 2010. V.98. P.1.

[6] Bodrov S.B., Ilyakov I.E., Shishkin B.V., Stepanov A.N. //Appl. Phys. Lett. 2012. V.100. P.201114.
[7] Bakunov M. I., Mashkovich E. A., Tsarev M. V., Gorelov S. D. //Appl. Phys. Lett. 2012. V.101. P.151102.

CONTRIBUTION OF SMALL WATER CLUSTERS IN HIGH TEMPERATURE WATER VAPOR SPECTRA

T.A. Odintsova[1)], M.Yu. Tretyakov[2)]

[1)]*Nizhny Novgorod State University*
[2)]*Institute of Applied Physics of RAS*

The general aim of this work is reveling the role of small water clusters in continuum atmospheric absorption. This work is continuation of research [1], where reanalysis of supercritical water vapor spectra in the O-H fundamental stretching region revealed manifestation of bound dimers and trimers. In the present work particular contributions of metastable dimers and trimes are also taken into account. For this analysis water vapor spectra in the range of 2500–5000 cm^{-1} recorded at 650 K and at pressures up to 130 atmospheres were used [2]. Water vapor is assumed to be a mixture of small water clusters. The total pressure is considered as a sum of partial pressures:

$$P = P_m + P_d + P_{dm} + P_t + P_{tm}, \quad (1)$$

where indexes *m*, *d*, *dm*, *t* and *tm* correspond to a monomer, a bound dimer, a metastable a dimer, a bound trimer and a metastable trimer respectively. In the model it was laid down, that the total integrated intensity (I) and the total absorption coefficient (α) are determined with the sum of contribution of a monomer, a dimer and a trimer, including their metastable states

$$\alpha(\nu) = \alpha_m(\nu) + \alpha_d(\nu) + \alpha_{dm}(\nu) + \alpha_t(\nu) + \alpha_{tm}(\nu) + \ldots, \quad (2)$$

$$I = I_m + I_d + I_{dm} + I_t + I_{tm} + \ldots \ , \quad (3)$$

While analyzing spectra we calculated the monomer contribution using HITRAN database parameters and taking into account the effect of line collisional coupling as in the work [1]. Bound dimer and trimer rovibration spectra were modeled on the basis of the data obtained from a cold molecular beam and He-droplet experiments. Metastable dimer and trimer contributions were taken into account by analogy with the work [3], namely the metastable dimer absorption was considered as a double monomer spectrum and metastable trimer absorption as a sum of bound dimer and monomer spectra. Dimer and trimer quantities were defined by corresponding equilibrium constants

$$P_d = K_d \cdot P_m^2, \quad P_{dm} = K_{dm} \cdot P_m^2, \quad P_t = K_t \cdot P_t^3, \quad P_{tm} = K_{tm} \cdot P_m^3, \quad (4)$$

which were considered to be variable coefficients in the expressions of the integrated intensity and the absorption coefficient as well as in the equation of water vapor thermodynamic state (1−3). Good agreement between the experimental data and the model function used was obtained. The determined values of equilibrium con-

stants (K_d=0.8·10^{-3} atm^{-1}, K_{dm}=1.1·10^{-3} atm^{-1}, K_t=3.3·10^{-6} atm^{-2} and K_{tm}=3.0·10^{-6} atm^{-2}) agree well with the estimation of the double and the triple molecule quantities in equilibrium water vapor (K_d=2.19·10^{-3} atm^{-1}, K_t=9.06·10^{-6} atm^{-2}) obtained from the high-precision hermodynamic water vapor data [4]. The analysis performed confirms the fact that the fraction of bound dimer and trimer is very significant even at the temperatures about their critical meanings.

The work is supported by RFBR.

[1] Tretyakov M.Yu., Makarov D.S. //J. of Chemical Physics. 2011. V.134. P.084306.
[2] Vigasin A.A., Jin Y., Ikawa S. //Molecular Physics. 2008. V. 106. P.1155.
[3] Ptashnik I.V., Shine K.P., Vigasin A.A. //J. of Quantitative Spectroscopy & Radiative Transfer. 2011. V. 112. P.1286.
[4] Tretyakov M.Yu., Serov E.A., Odintsova T.A. //Radiophysics and Quantum Electronics. 2012. V. 54. P.700.

DIAGNOSTICS OF PLASMA IN LWFA EXPERIMENTS AT PEARL FACILITY

K.F. Burdonov, A.A. Soloviev

Institute of Applied Physics of RAS

When the petawatt-level-power laser pulse is focusing into the gas jet target, effective acceleration of plasma background electrons to energies of hundreds MeV at centimeter scale takes place through the laser wakefield acceleration (LWFA) mechanism [1, 2]. Experiments at PEARL facility, employing OPCPA technology [3], are aimed to electron acceleration in plasma through LWFA. For creating optimal electron acceleration conditions one need to know most every input parameter of laser radiation and plasma conditions. This paper is devoted to direct and indirect diagnostics of plasma density concentration in LWFA experiments at PEARL facility.

Experimental scheme of laser-plasma electron acceleration at PEARL facility is shown on Fig. 1. For detailed description of laser-plasma experiments and diagnostic at PEARL see Ref. 4 and 5. In short the main PEARL pulse is split into two parts by the transparent mirror before the interaction vacuum chamber, where laser-plasma interaction takes place. The powerful pulse then serves as a driver coming into the target chamber where it is focused into a supersonic gas jet by means of an off-axis parabolic mirror with *f*/15 or *f*/6 forming the focal spot sizes of the laser beam of 18 μm and 7.2 μm at FWHM intensity, respectively. The average laser intensities correspond to the normalized vector potential a_0 = 2 and a_0 = 7, respectively. The second part with a much lower power transmitted by the mirror comes

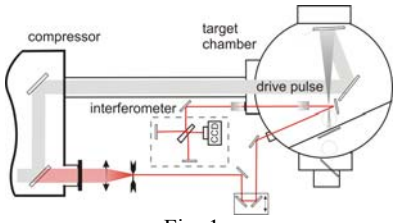

Fig. 1

into the diagnostic channel where it is used for the diagnostics, including the interferometric diagnostic of plasma density. Helium or nitrogen gas jet is formed with a specially designed supersonic conical nozzle with diameters of 2 mm, 5 mm, and 10 mm.

Indirect measurement consists of gas jet calibration for three different nozzle diameters (2, 5 and 10 mm) for helium and nitrogen gases in the range of backing pressure from 5 to 100 bar. Measurement of gas density is performed by means of Michelson interferometer in one arm of which the gas jet is placed. The interference patterns are registered by a CCD camera. The inverse Abel transformation is also applied to the gas jet induced phase distortions to reconstruct the gas density profile. The calibration shows that the nozzles produce flat-top gas density profiles with a plateau size of 1 mm, 3.5 mm and 8 mm for the 2, 5 and 10 mm diameter nozzles, respectively. A typical jet induced phase distortion and density profile at 1 mm above the nozzle edge for 10 mm nitrogen gas jet at 100 bar of backing pressure are presented in Fig. 2 (a, b). The calibration shows that the value of gas density depends linearly on the nozzle backing pressure for the range of 5 to 100 bar.

Direct measuring of plasma density taking place during the LWFA experiments, also performs by means of the Michelson interferometer (Fig. 1). The probe radiation that is a weaker femtosecond replica of the high-power pulse allows temporal resolution of the phase measurements on a femtosecond time scale. It should be noted that using this technique plasma density distribution can be measured correctly, if the plasma channel has axial symmetry. In fact, in a He gas jet the measured plasma density exceeds neutral density by a factor of 2, which means that He is fully ionized. This is in a good agreement with the fact that at the laser intensities of order 10^{19} W/cm^2 used in the experiment He gas should be fully ionized [6]. However, for N_2 gas jet the ionization degree depends on laser intensity and, hence, the plasma channel is strongly nonuniform in radial direction. Full ionization of nitrogen occurs only at laser intensities exceeding 10^{19} W/cm^2 [7]. According to this paper we expect five times ionized nitrogen for the focusing angle *f*/15 and fully stripped nitrogen plasma in experiment with *f*/6 focusing mirror. The resulting observations are presented in Fig. 2 (c, d). One can see a plasma channel with the corresponding plasma density $N_e = 7\times10^{18}$ cm^{-3} measured at 30 bar backing pressure and *f*/15 focusing.

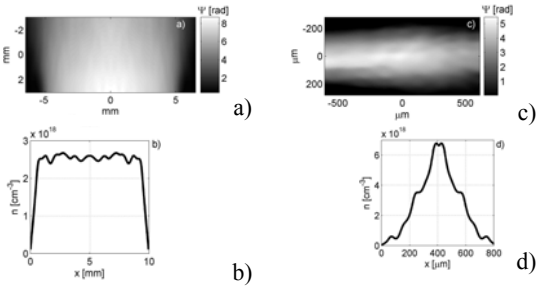

Fig. 2

The neutral density N and the corresponding plasma density N_e for different nozzles at 10 bar backing pressure are given in Table.

Tabl.

Nozzle diameter	N / N_e [1/cm^3], He	N / N_e(f/6) / N_e(f/15) [1/cm^3], N_2
2 mm	$1.8 \cdot 10^{18} / 3.6 \cdot 10^{18}$	$1.8 \cdot 10^{18} / 2.5 \cdot 10^{19} / 1.8 \cdot 10^{19}$
5 mm	$1.75 \cdot 10^{18} / 3.5 \cdot 10^{18}$	$1.5 \cdot 10^{18} / 2.1 \cdot 10^{19} / 1.5 \cdot 10^{19}$
10 mm	$2.5 \cdot 10^{17} / 5 \cdot 10^{17}$	$2.5 \cdot 10^{17} / 3.5 \cdot 10^{18} / 2.5 \cdot 10^{18}$

Direct and indirect measurements of plasma density profiles in LWFA experiments on PEARL facility are performed. Calibration plasma density quantities for nozzles 2, 5 and 10 mm for nitrogen and helium for *f*/6 and *f*/15 focusing are obtained. Accelerated electron bunches with energies up to 300 MeV are achieved at this range of plasma concentration [6].

[1] Kneip S., Nagel S. et al. // Phys. Rev. Lett. 2009. V.103. P.035002.
[2] Froula D., Clayton C. et al. // Phys. Rev. Lett. 2009/ V.103. P.215006.
[3] Lozhkarev V., Freidman G. et al. // Laser Phys. Lett. 2007. V.4(6). P.421.
[4] B. Walker, B. Sheehy et al. // Phys. Rev. A. 1993. V.48. P.R894.
[5] S. Hulin, T. Auguste et al. // Phys. Rev. E. 2000. V.61. P.5693.
[6] Soloviev A., Burdonov K. et al. // Nucl. Instr. & Meth. Phys. Res A. 2011. V.653(1). P.35.